NASA/TM—2002–211616

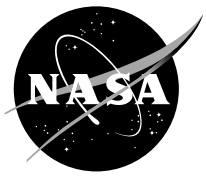

Subtropical Gyre Variability Observed by Ocean Color Satellites

C.R. McClain
S.R. Signorini
J.R. Christian

National Aeronautics and
Space Administration

Goddard Space Flight Center
Greenbelt, Maryland 20771

September 2002

The NASA STI Program Office … in Profile

Since its founding, NASA has been dedicated to the advancement of aeronautics and space science. The NASA Scientific and Technical Information (STI) Program Office plays a key part in helping NASA maintain this important role.

The NASA STI Program Office is operated by Langley Research Center, the lead center for NASA's scientific and technical information. The NASA STI Program Office provides access to the NASA STI Database, the largest collection of aeronautical and space science STI in the world. The Program Office is also NASA's institutional mechanism for disseminating the results of its research and development activities. These results are published by NASA in the NASA STI Report Series, which includes the following report types:

- TECHNICAL PUBLICATION. Reports of completed research or a major significant phase of research that present the results of NASA programs and include extensive data or theoretical analysis. Includes compilations of significant scientific and technical data and information deemed to be of continuing reference value. NASA's counterpart of peer-reviewed formal professional papers but has less stringent limitations on manuscript length and extent of graphic presentations.
- TECHNICAL MEMORANDUM. Scientific and technical findings that are preliminary or of specialized interest, e.g., quick release reports, working papers, and bibliographies that contain minimal annotation. Does not contain extensive analysis.
- CONTRACTOR REPORT. Scientific and technical findings by NASA-sponsored contractors and grantees.
- CONFERENCE PUBLICATION. Collected papers from scientific and technical conferences, symposia, seminars, or other meetings sponsored or cosponsored by NASA.
- SPECIAL PUBLICATION. Scientific, technical, or historical information from NASA programs, projects, and mission, often concerned with subjects having substantial public interest.
- TECHNICAL TRANSLATION. English-language translations of foreign scientific and technical material pertinent to NASA's mission.

Specialized services that complement the STI Program Office's diverse offerings include creating custom thesauri, building customized databases, organizing and publishing research results . . . even providing videos.

For more information about the NASA STI Program Office, see the following:

- Access the NASA STI Program Home Page at http://www.sti.nasa.gov/STI-homepage.html
- E-mail your question via the Internet to help@sti.nasa.gov
- Fax your question to the NASA Access Help Desk at (301) 621-0134
- Telephone the NASA Access Help Desk at (301) 621-0390
- Write to:
  NASA Access Help Desk
  NASA Center for AeroSpace Information
  7121 Standard Drive
  Hanover, MD 21076–1320

NASA/TM—2002–211616

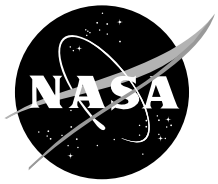

Subtropical Gyre Variability Observed by Ocean Color Satellites

Charles R. McClain
Goddard Space Flight Center
Greenbelt, Maryland

Sergio R. Signorini
Science Applications International Corporation
Beltsville, MD

James R. Christian
Earth System Science Interdisciplinary Center
University of Maryland
College Park, MD

National Aeronautics and
Space Administration

Goddard Space Flight Center
Greenbelt, Maryland 20771

September 2002

Acknowledgements

The authors would like to thank the NASA Ocean Biogeochemistry program for its support of this research. We greatly appreciate the efforts of the NASA ocean altimetry pathfinder activity which provided the TOPEX/Poseidon data products, NASDA and the NASA SIMBIOS Project which collaborated on the generation of the OCTS data products, and the NASA SeaWiFS Project and Orbital Image Corporation (OrbImage) for the SeaWiFS data products.

Available from:

NASA Center for AeroSpace Information
7121 Standard Drive
Hanover, MD 21076–1320
Price Code: A17

National Technical Information Service
5285 Port Royal Road
Springfield, VA 22161
Price Code: A10

Prologue

The subtropical gyres of the world are extensive, coherent regions that occupy about 40% of the surface of the earth. Once thought to be homogeneous and static habitats, there is increasing evidence that mid-latitude gyres exhibit substantial physical and biological variability on a variety of time scales. While biological productivity within these oligotrophic regions may be relatively small, their immense size makes their total contribution significant. Global distributions of dynamic height derived from satellite altimeter data, and chlorophyll concentration derived from satellite ocean color data, show that the dynamic center of the gyres, the region of maximum dynamic height where the thermocline is deepest, does not coincide with the region of minimum chlorophyll concentration. The physical and biological processes by which this distribution of ocean properties is maintained, and the spatial and temporal scales of variability associated with these processes, are analyzed using global surface chlorophyll-a concentrations, sea surface height, sea surface temperature and surface winds from operational satellite and meteorological sources, and hydrographic data from climatologies and individual surveys. Seasonal and interannual variability in the areal extent of the subtropical gyres are examined using 8 months (November 1996 - June 1997) of OCTS and nearly 5 years (September 1997 - June 02) of SeaWiFS ocean color data and are interpreted in the context of climate variability and measured changes in other ocean properties (i.e., wind forcing, surface currents, Ekman pumping, and vertical mixing). The North Pacific and North Atlantic gyres are observed to be shrinking over this period, while the South Pacific, South Atlantic, and South Indian Ocean gyres appear to be expanding.

Table of Contents

Introduction

The subtropical gyres of the world are extensive, coherent regions that occupy ~40% of the surface of the earth. The upper kilometer of the subtropical gyres is primarily wind driven (Huang and Russell, 1994). The horizontal and vertical motion in this layer plays a significant role in controlling the interaction between the atmosphere and ocean, which is of vital importance to our understanding of the oceanic general circulation and climate (Huang and Qiu, 1994). The gyres are characterized by a deep pycnocline at their centers and strong horizontal gradients of temperature (T) and salinity (S) at the fringes due to pycnocline outcropping. The flow in the western limbs (western boundary currents) is intensified by the latitudinal changes of the Coriolis acceleration (β effect), while the flow is relatively weak in the gyres' eastern parts. The broad region of relatively weak flow occupies most of the gyre and is called the Sverdrup regime (Pedlosky, 1990). The dynamic center of the gyres can be identified by a maximum sea surface height (SSH) where the Ekman flow converges and the thermocline subsides via Ekman downwelling. The thermocline shoals in the mid-latitudes, where thermocline isopycnals outcrop at the surface, and at the equator, where Ekman flow divergence promotes upwelling. These two regions define the north and south limbs of the subtropical gyres, respectively.

From a biological standpoint, the interior of the subtropical gyres are regions where nutrient supply to the euphotic zone (~100 m) is minimal and concentrations of nutrients and biomass are relatively low throughout the year. While biological productivity within the oligotrophic regions of the gyres may be relatively small (Hayward, 1987; 1991; Jenkins and Goldman, 1985; Jones *et al.*, 1996; Karl *et al.*, 1996), their immense size makes their total contribution significant. An important biological characteristic of the subtropical gyres is the large variability in phytoplankton growth rates with minimal changes in biomass (Laws *et al.*, 1987; Marañón *et al.*, 2000; Marra and Heinemann, 1987). Understanding the interactions between physical and biological processes within the subtropical gyres is central for determining the magnitude and variability of the carbon exported from the surface to the deep ocean.

Once thought to be homogeneous and static habitats, there is increasing evidence that subtropical gyres exhibit substantial physical and biological variability on a variety of time scales (Karl and Lukas, 1996). Ecosystem indicators in the subtropical gyres, such as biomass, chorophyll-a (chl-*a*) concentration, and new and export productions, respond to climate variability (Karl *et al.*, 2001; Oschlies, 2001). This physical-biological coupling between the climate cycles, e.g., El Niño-Southern Oscillation (ENSO), the Pacific Decadal Oscillation (PDO), the North Atlantic Oscillation (NAO) and the Antarctic Circumpolar Wave (ACW), and ecosystem dynamics is a consequence of altered nutrient flux pathways that result from changes in the stratification and circulation of the subtropical gyres. Climate-induced variations in community structure and biogeochemical processes of the North Pacific subtropical gyre (Karl *et al.*, 2001) and the North Atlantic (Ottersen *et al.*, 2001) have been linked the PDO and NAO, respectively. A more complete discussion of these modes of climate variability and their effects on marine ecosystems is provided in the Appendix.

This paper examines five major gyre systems, i.e., the North and South Pacific, the North and South Atlantic, and the southern Indian Ocean, and provides brief initial analyses of the relationship between gyre physics (dynamics and hydrographic structure) and surface biology as observed in satellite ocean color imagery, the seasonal cycle of forcing and upper ocean phytoplankton response within the gyres, and the observed interannual trends in the

oligotrophic gyre spatial extents and mean chl-*a* concentrations. Some inferences regarding the couplings between the gyre ecosystems and physical forcings (circulation, hydrography, and climate variability) are suggested, but more definitive discussions will need to be based on longer satellite ocean color time series and modeling studies.

Data Sources

The main data set for this study is a 5-year time series of ocean color global monthly composites originating from the Japanese Ocean Color and Temperature Sensor (OCTS; 8 months) and Sea-viewing Wide-Field-of-View Sensor (SeaWiFS; 58 months) satellite sensors. The OCTS data products used for the analysis were at NASA Goddard Space Flight Center (GSFC) as part of a joint NASDA-NASA collaboration. The products are available from the GSFC Sensor Intercomparison and Merger for Biological and Interdisciplinary Oceanic Studies (SIMBIOS) Project. The OCTS reprocessing used atmospheric correction and bio-optical algorithms comparable to those used for SeaWiFS. Both the OCTS and SeaWiFS data sets used a Marine Optical Buoy (MOBY)-based vicarious calibration (Eplee *et al.*, 2001; Wang *et al.*, 2002). Prior to the derivation of the vicarious calibration adjustments to the prelaunch SeaWiFS calibration, sensor degradation is removed using a time series of monthly lunar images collected at about the same lunar phase angle (Barnes *et al.*, 1999; Barnes *et al.*, 2001). The lunar calibration results in a very accurate characterization of the sensor stability. The SeaWiFS data is from reprocessing #4 which was completed in July 2002 (see the SeaWiFS homepage for more information). In situ data for validation of chl-*a* retrievals inside the most oligotrophic regions of the gyres are sparse, e.g., the western North Pacific and the southern hemisphere gyres. However, sections from the World Ocean Circulation Experiment (WOCE) and occasional cruises into these regions are available, e.g., the South Pacific (Chavez *et al.*, 1995).

Other ancillary data sets were used in the analyses including the Reynolds and Smith (1994) SST monthly products, the T/P SSH anomaly (SSHA) monthly grids (GSFC Ocean Pathfinder database), Ekman vertical velocities derived from NCEP winds, climatological T, S, nitrate concentration, and mixed layer depth (National Ocean Data Center Ocean Atlas 1998), and three-year (1998-2000) monthly averaged photosynthetically available radiation (PAR) derived from SeaWiFS (unpublished algorithm by Robert Frouin and others).

Results and Discussion

Offset Between the Dynamic and Biological Gyre Centers

In many areas, such as upwelling regimes, the surface topography is correlated with the thermocline depth and, therefore, the nutricline. This correlation has been used by Turk *et al.* (2001), for instance, to infer new production in the equatorial Pacific. However, the dynamic center of the gyres does not coincide with the "biological" center of the gyres, i.e., the region of minimum surface chlorophyll-a (chl-*a*) concentration as derived from the SeaWiFS data set. Figure 1 shows color plates of the global dynamic height (December 1997 - December 2000) derived from TOPEX/Poseidon (T/P) SSH and global surface chl-*a* concentration from SeaWiFS (average of January 1998 - December 2000). The gyres are highlighted by the white boxes, which also delimit the regions to be analyzed.

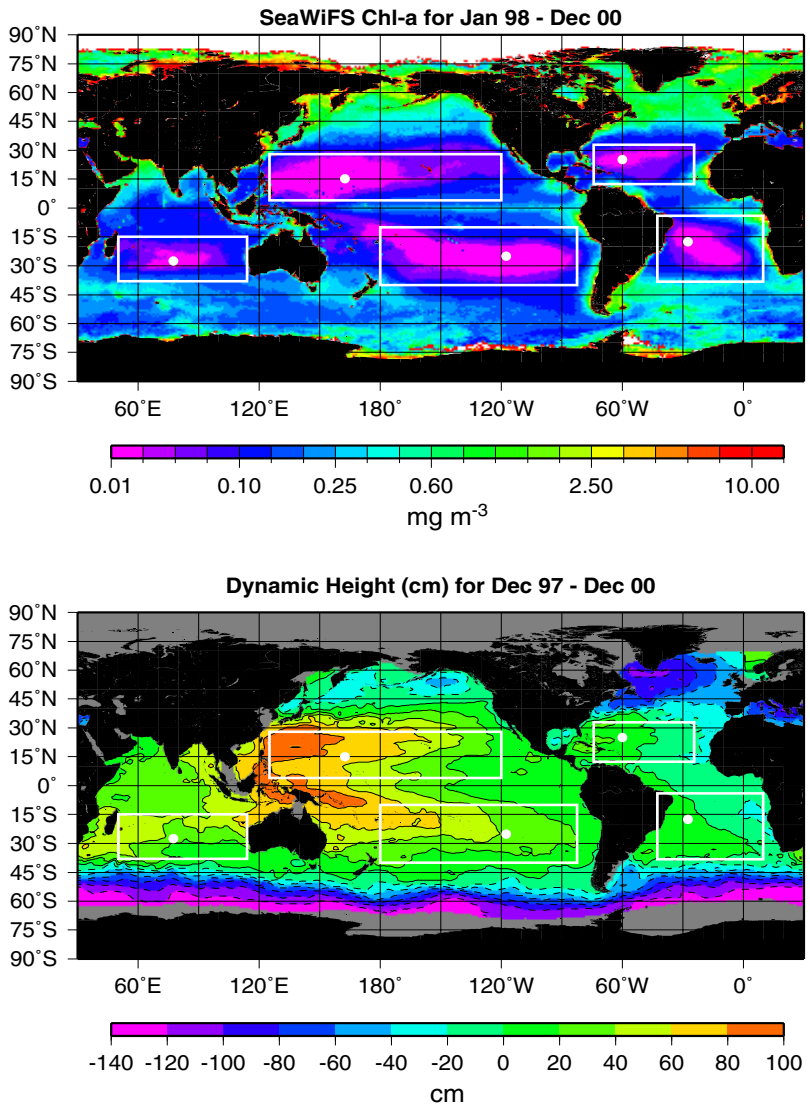

Fig. 1. Global distribution of chlorophyll concentration (top) derived from a January 1998 - December 2000 SeaWiFS composite, and global distribution of dynamic height (bottom) derived from TOPEX/Poseidon altimeter data (December 19997 - December 2000) and climatological hydrography. The level of reference for the dynamic height is 2250 meters. The white dots show the location of the minimum chlorophyll concentration. The boxes delimited by the black lines represent the areas of each gyre to be used in the data analysis.

The location of minimum surface chl-*a* concentration is indicated for each gyre by the white dots. Clearly, the minimum chl-*a* concentration does not coincide with the dynamic centers of the gyres (maximum dynamic height and depressed thermocline), especially in the Pacific where the distance between the dynamic and biological gyre centers for the North Pacific and South Pacific is 3400 km and 9200 km, respectively. This pattern is counter-intuitive because the location of the maximum dynamic height is an indication of maximum thermocline depth and, presumably, the deepest nutricline. The correspondence between the thermocline and the nutricline does vary for a variety of reasons, e.g., the origin of the source water and differing time scales of local physical and biological processes. However, to the first order, this

apparent discrepancy can be explained by the dynamical behavior of the gyres as exemplified by the North and South Pacific gyres.

Kleeman *et al*. (2000) showed that the observed subtropical North Pacific gyre circulation has a shift in meridional location with depth. At shallow levels (~100 m), the gyre center, identified as the minimum density and highest sea level, is at approximately 15°N. The gyre center is shifted northward at deeper depths; ~22°N at 300 m, and ~30°N below 400 m. Using analytical solutions of the beta-plane shallow water equations, Kleeman *et al*. (2000) argued that such a shift can be explained by the effects of oceanic dissipation processes. The highly damped solution is proportional to Ekman pumping (downward velocity), while the lightly damped case tends toward the classical Sverdrup solution. The Ekman pumping peaks near 15°N while the Sverdrup solution for pressure peaks at 30°N. They demonstrated that there are two factors that explain the observed shift in the North Pacific subtropical gyre. First, density deviations in the upper ocean are more strongly influenced by higher order baroclinic modes than those in the deep ocean, which are influenced by the lower modes. Second, dissipation processes act much more strongly on the higher order baroclinic modes because of their slower speeds and smaller Rossby radii. In terms of biological response, the chl-*a* minimum (Figure 2) is located at the latitude of the peak Ekman downwelling (minimum w_e) near 15°N, the upper-ocean gyre center where the nutricline is deepest (Figure 2).

Of the gyre systems, the South Pacific gyre is the most distinct (Morris *et al.*, 1996), because the boundary current, recirculation zone, and quiescent eastern regions are more clearly separated due to the large area of the South Pacific Ocean. Also, this gyre has the largest shift in location with depth, but the dissipation effect may not be the main cause of the shift in meridional location with depth. Instead, surface heat and freshwater fluxes may play a major role in the shift. As shown in Figure 1, the observed maximum dynamic height (near 5°S, 160°E) is located in the relatively shallow Warm Pool where the density deviation peaks due to the warm and fresh waters occupying that site. Figure 2 shows 3-year composites of dynamic height and geostrophic currents (top plate), SeaWiFS chl-*a* (bottom plate), and the depth of the climatological 2 μM nitrate (middle plate) isopleth. The spatial distribution of the 2 μM nitrate isopleth indicates that the maximum nutricline depth and the minimum chl-*a* concentration are located at approximately 25°S, 118°W.

Figures 3 and 4 show the subsurface hydrography and nitrate distribution along the major and minor axes of the gyre (perpendicular white lines in Figure 2), respectively. Figure 3 shows T, S, density, nitrate, and geostrophic current transects along the major axis of the South Pacific gyre. The high salinity core is a result of water vapor divergence out of the subtropical high (Chen *et al.*, 1994). The vectors along the surface of the temperature transect represent the Ekman vertical velocity, indicating that there is downwelling on the southeast (SE) side and upwelling on the northwest (NW) side at the Warm Pool. There is a secondary northwestward flow that ensues, which can be traced by the spreading of the high salinity core. This secondary flow tilts the gyre axis towards the NW within the upper 250 meters. The two wide arrows indicate the positions of the minimum chl-*a* and the gyre center, i.e., where the geostrophic surface flow reverses. The chl-*a* minimum coincides with the crossover of the zero velocity contour and the 4 μM nitrate contour at ~250 m, and corresponds to the location of the deepest nutricline. Figure 4 shows the equivalent transects for the minor axis

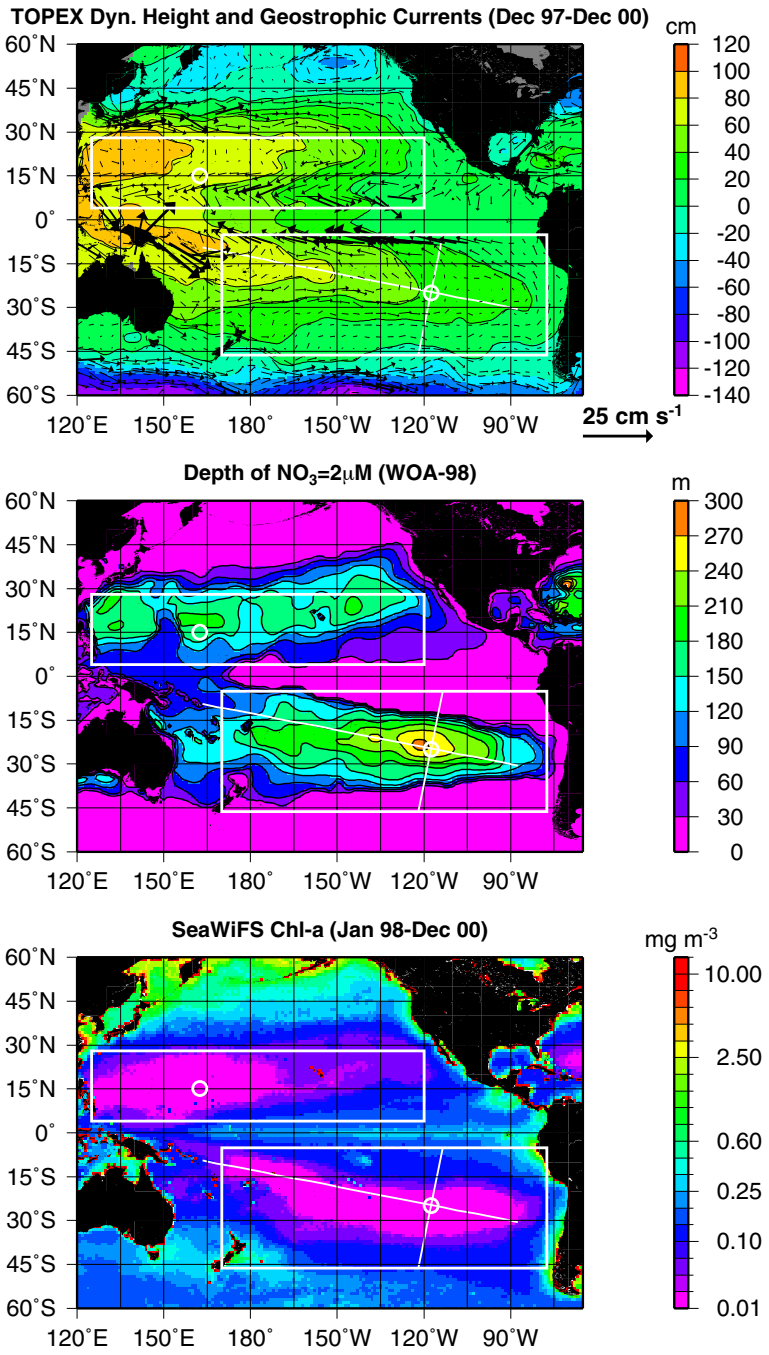

Fig. 2. Three-year composites of dynamic height and geostrophic currents derived from T/P SSH (top plate), depth of the 2 μM nitrate concentration (middle plate), and SeaWiFS chlorophyll (bottom panel). The white rectangles delimit the analysis regions of the North and South Pacific gyres and the white cicles represent the locations of the minimum chlorophyll concentration. The two perpendicular lines represent the major and minor axis of the South Pacific subtropical gyre.

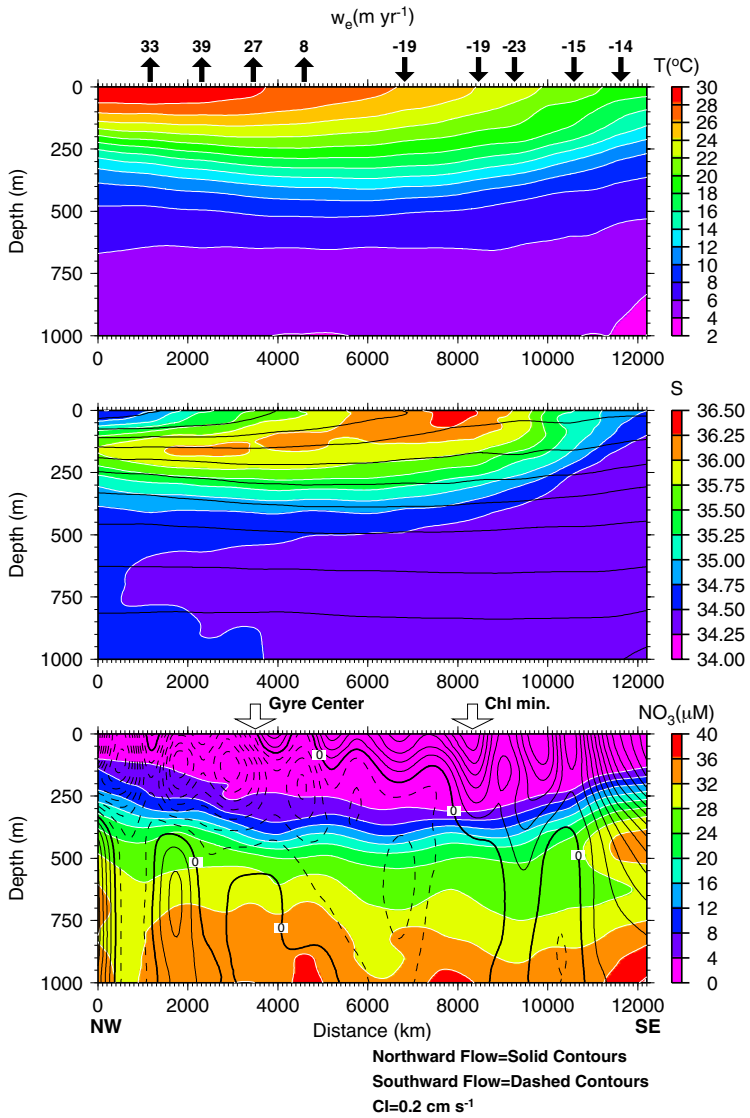

Fig. 3. Transects of temperature (top plate), salinity (middle plate), and nitrate (bottom plate) along the major axis of the South Pacific subtropical gyre. The arrows along the top of the temperature transect represent the climatological Ekman suction (upwelling) and Ekman pumping (downwelling). The black contours superimposed on the salinity transect are the climatological in situ density (values not shown). The density contours range from 22 to 32 kg m^{-3} at 1 kg m^{-3} intervals. The black contours (solid=positive, dashed=negative) superimposed on the nitrate transect represent the geostrophic flow (1500 m reference level); the large arrows at the surface indicate the locations of the surface gyre center and the chlorophyll minimum, which is collocated with the deepest nutricline.

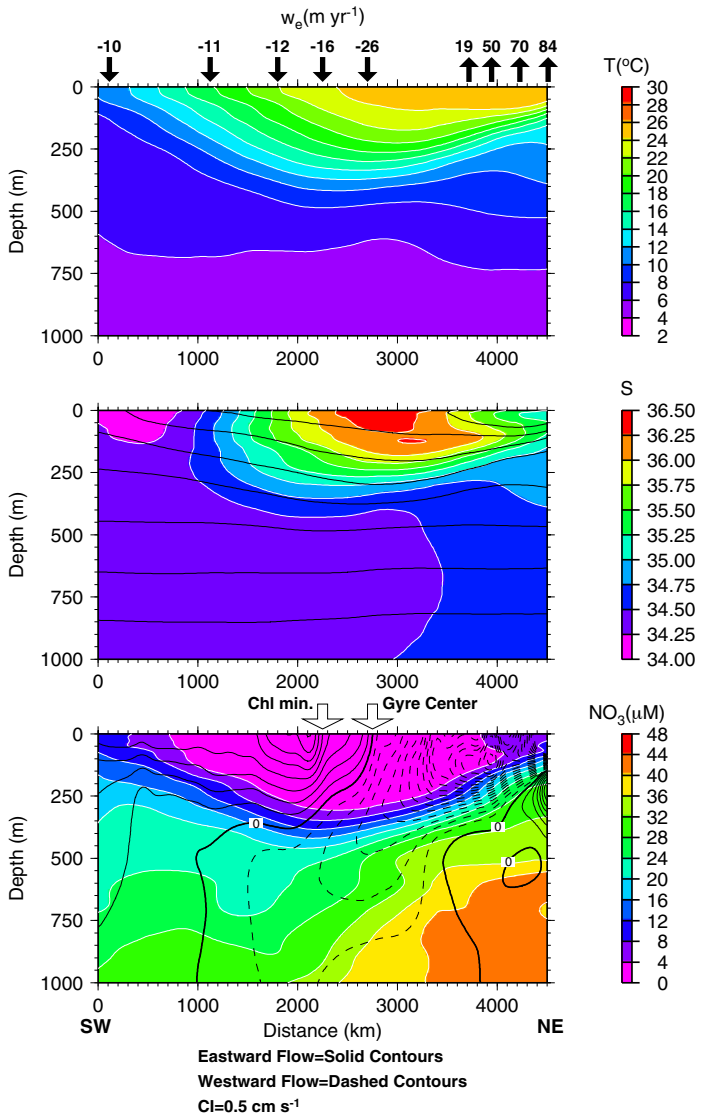

Fig. 4. Transects of temperature (top plate), salinity (middle plate), and nitrate (bottom plate) along the minor axis of the South Pacific subtropical gyre. The arrows along the top of the temperature transect represent the climatological Ekman suction (upwelling) and Ekman pumping (downwelling). The black contours superimposed on the salinity transect are the climatological in situ density (values not shown). The density contours range from 24 to 31 kg m^{-3} at 1 kg m^{-3} intervals. The black contours (solid=positive, dashed=negative) superimposed on the nitrate transect represent the geostrophic flow (1500 m reference level); the large arrows at the surface indicate the locations of the surface gyre center and the chlorophyll minimum, which is collocated with the deepest nutricline.

of the South Pacific gyre. The same secondary flow pattern and the tilt of the gyre axis are evident in these transects. Finally, Ekman pumping peaks near 25°S, 118°W, the location of minimum chl-*a* concentration and deepest nutricline (~300 m).

Seasonal Cycle of Physical Forcing and Biological Response

The seasonal circulation in the subtropical gyres is driven by seasonal changes in the wind field. This seasonal strengthening and weakening of the gyres causes vertical displacement of the thermocline and nutricline as a response to baroclinic adjustment and Ekman pumping. The biological response to the nutricline vertical displacement is a corresponding seasonal change in the size and location of the oligotrophic regions of the subtropical gyres. This is evident in Figure 5, which shows seasonal climatology from the first four years of SeaWiFS chl-*a* concentrations. The white circles indicate the climatological location of the chl-*a* minimum. The white boxes delimit the analysis regions and the white contours indicate the 0.07 mg m^{-3} chl-*a* concentration, which are used hereafter to determine the size of the oligotrophic regions of the gyres. In the southern hemisphere gyres, the maximum contraction of the oligotrophic area, or the maximum chl-*a* concentration, occurs in the austral winter. Alternatively, the maximum expansion of the oligotrophic areas occurs in austral summer. The northern hemisphere subtropical gyres have the opposite phasing with respect to the seasons.

The seasonal global distribution of the climatological depth of the 2 μM nitrate concentration (ZNO_3) is shown in Figure 6. The minimum chl-*a* concentration is usually near the deepest ZNO_3, indicating that the interior regions of the subtropical gyres are nutrient limited throughout the year, although other nutrients, i.e., phosphate and Fe, may be limiting as well. Artifacts due to poor in situ coverage are apparent in some locations, e.g., the western North Pacific near 15°N.

The seasonal cycle of physical forcing and biological responses for the North Pacific, South Pacific, Indian Ocean, North Atlantic, and South Atlantic gyres are shown in Figure 7. The time series plots are area averages (Figure 1) of w_e, PAR, MLD, SST, SSHA, and the fraction of pixels (A_{chl}) inside the study regions with chl ≤ 0.07 mg m^{-3}. Of these parameters, the mean Ekman upwelling appears to be unique for each gyre in terms of the shape and amplitude of the seasonal cycle.

In the North Pacific gyre, the largest A_{chl}, corresponding to the minimum chl-*a* concentration, occurs in September, the trade wind minimum (Wyrtki and Meyers, 1976), when the thermocline is deepest, downwelling is maximum, and the MLD is shallowest. The smallest A_{chl}, corresponding approximately to the maximum regionally-average chl-*a* concentration, occurs in January when the thermocline is shallowest, upwelling is near maximum, and the MLD is deepest (~70 m). Therefore, the seasonal variability of the size of the oligotrophic region is driven by a combination of mixing (as indicated by the MLD), downwelling, and thermocline displacement.

The fractional size of the South Pacific gyre reaches a minimum in July-August as the mixed layer approaches its greatest depth in September. Downwelling is weakest from March through September. The SSHA decreases from April through October, indicating a steady upward displacement of the thermocline. Vertical mixing seems to be the predominant factor driving the changes in the size of the oligotrophic region in the South Pacific gyre.

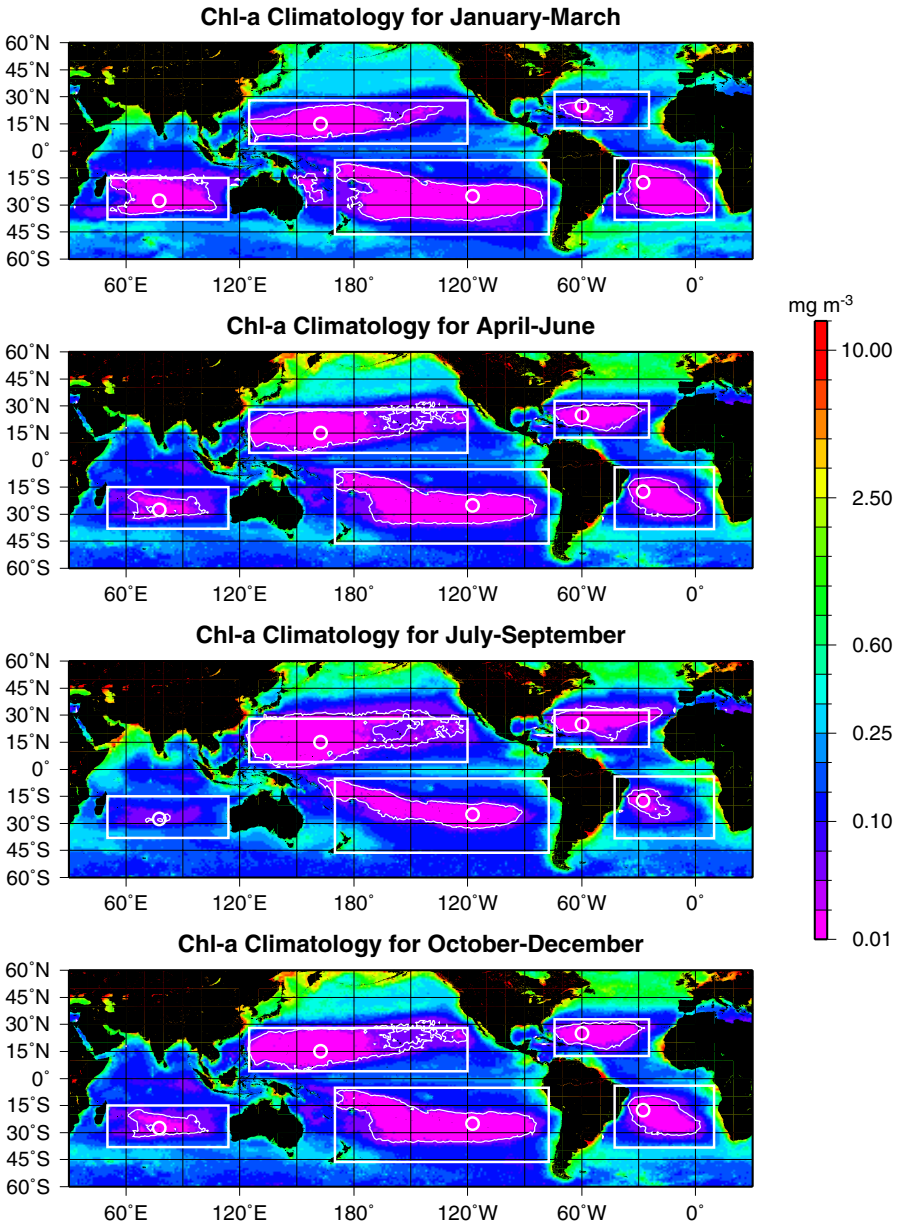

Fig. 5. Global distribution (60^{o}S - 60^{o}N) of seasonal chlorophyll concentration from SeaWiFS. The white boxes are the gyre regions used for analysis and the white circles indicate the location of the chlorophyll minimum. The white contours represent the 0.07 mg m^{-3} chlorophyll concentration. Note the seasonal expansion and contraction of the contours.

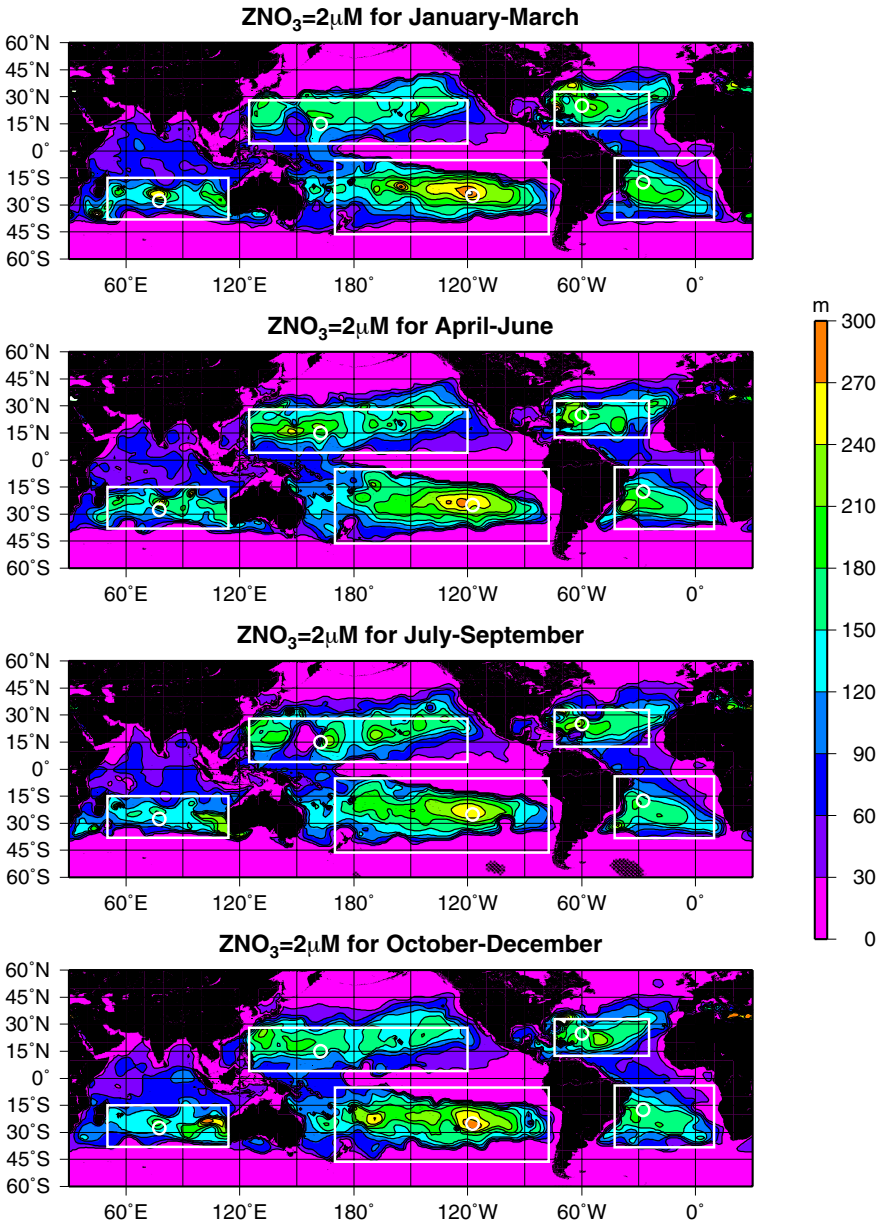

Fig. 6. Global distribution (60°S - 60°N) of seasonal nutricline depth, defined as the depth of the 2 μM nitrate concentration (ZNO_3), derived from World Ocean Atlas 98. The white boxes are the gyre regions used for analysis and the white circles indicate the location of the chlorophyll minimum. Note that the locations of the chlorophyll minimum are near the deepest nutricline.

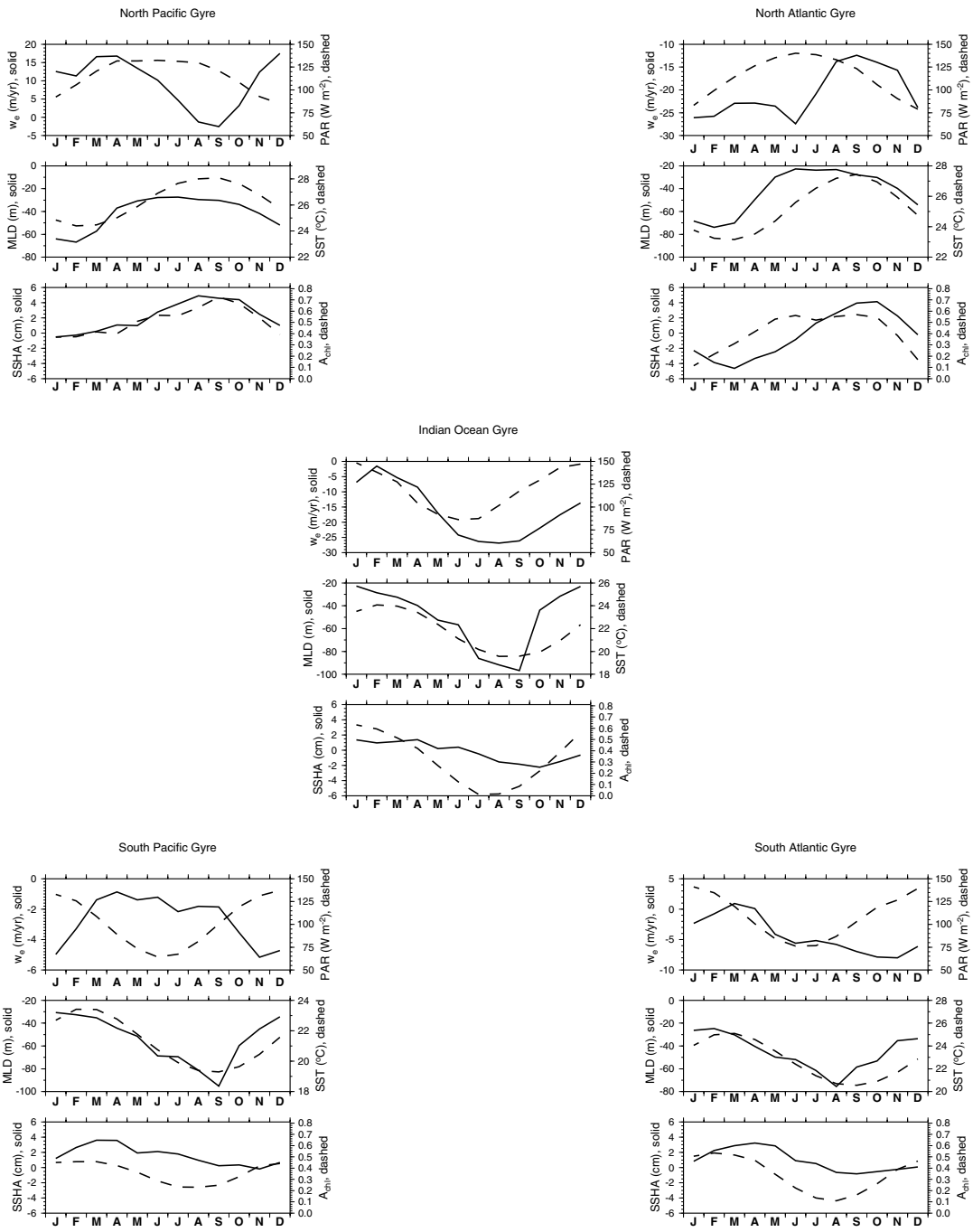

Fig. 7. Seasonal cycle of forcing and response for the North Pacific, South Pacific, Indian Ocean, North Atlantic, and South Atlantic subtropical gyres. Each of the three tiers show the seasonal variability of Ekman vertical velocity (solid line), three-year (1998-2000) monthly average of SeaWiFS PAR (dashed line), mixed layer depth (solid line), SST (dashed line), SSHA (solid line), and the gyre fractional area (A_{Chl}) with chlorophyll concentration less than 0.07 mg m^{-3} (dashed line).

The central South Pacific gyre has the lowest chl-*a* concentration of the global oceans. Figure 8 shows a time series of OCTS and SeaWiFS chlorophyll, PAR, and SST-derived MLD at 28°S, 105°W (solid line). An analytical expression for MLD was obtained from a linear correlation with climatological SST (r^2=0.72). The interannual MLD time series was computed using the analytical expression and monthly SST values (Reynolds and Smith, 1994). The time series for equivalent parameters at the location of the minimum chl-*a* (25°S, 117.5°W) inside the gyre (dashed line) are also plotted for comparison. The March 1994 chlorophyll value (~0.02 mg m^{-3}) observed by Chavez *et al.* (1995) at 28°S, 105°W is repeated every year on the time series for comparison (shown by the black triangles). The largest chl-*a* values in the time series (marked by the vertical dashed lines in Figure 8) occur during the austral winter when the mixed layer is deep and the phytoplankton produce more chlorophyll in response to photoadaptation to lower light levels imposed by deeper mixing. This chlorophyll response to photoadaptation has been demonstrated in the North Pacific gyre (Winn *et al.*, 1995). Photoadaptation in the highly oligotrophic regions of the gyres is the most probable cause of chl-*a* enhancement since winter nutrient renewal in the euphotic zone is limited because the nutricline (Figure 6) is much deeper than the mixed layer (<100 m).

Similar descriptions can be outlined for the Atlantic gyres. The North Atlantic gyre is characterized by maximum downwelling between January and June. The MLD shallows rapidly during March through May and generally leads SST. SSHA is most negative in March and most positive during September-October. A_{chl} is minimal in December-January and has a broad maximum during May-October. In the South Atlantic, downwelling is strongest in October-November. The MLD is deepest in August and generally leads SST. SSHA is relatively flat compared to the North Atlantic. Finally, the South Atlantic and South Pacific gyres have strikingly similar cycles of forcing, except for Ekman downwelling, and responses.

In the Indian Ocean, the fractional size of the oligotrophic region of the gyre is directly correlated with downwelling intensity (Figure 7). This means that, as downwelling gets stronger, the chlorophyll concentration increases. This biological response to the physical forcing is counterintuitive. A plausible explanation for this apparent discrepancy will be offered later in this section through further analysis. The North Atlantic and South Atlantic gyres have biological responses consistent with the MLD, SSHA, and w_e seasonal forcing.

The cross-correlation and lag between A_{chl} and MLD, SST, SSHA, and w_e for all five gyres are summarized in Table 1. This table shows cross-correlation and lag in months between the fractional size of the oligotrophic area and the physical forcing for all gyres. The correlation coefficients are fairly large for all variables and quantify the conclusions discussed above. The sign of the correlation coefficients are consistent with the biological response to physical forcing as outlined above, except for the Indian Ocean gyre.

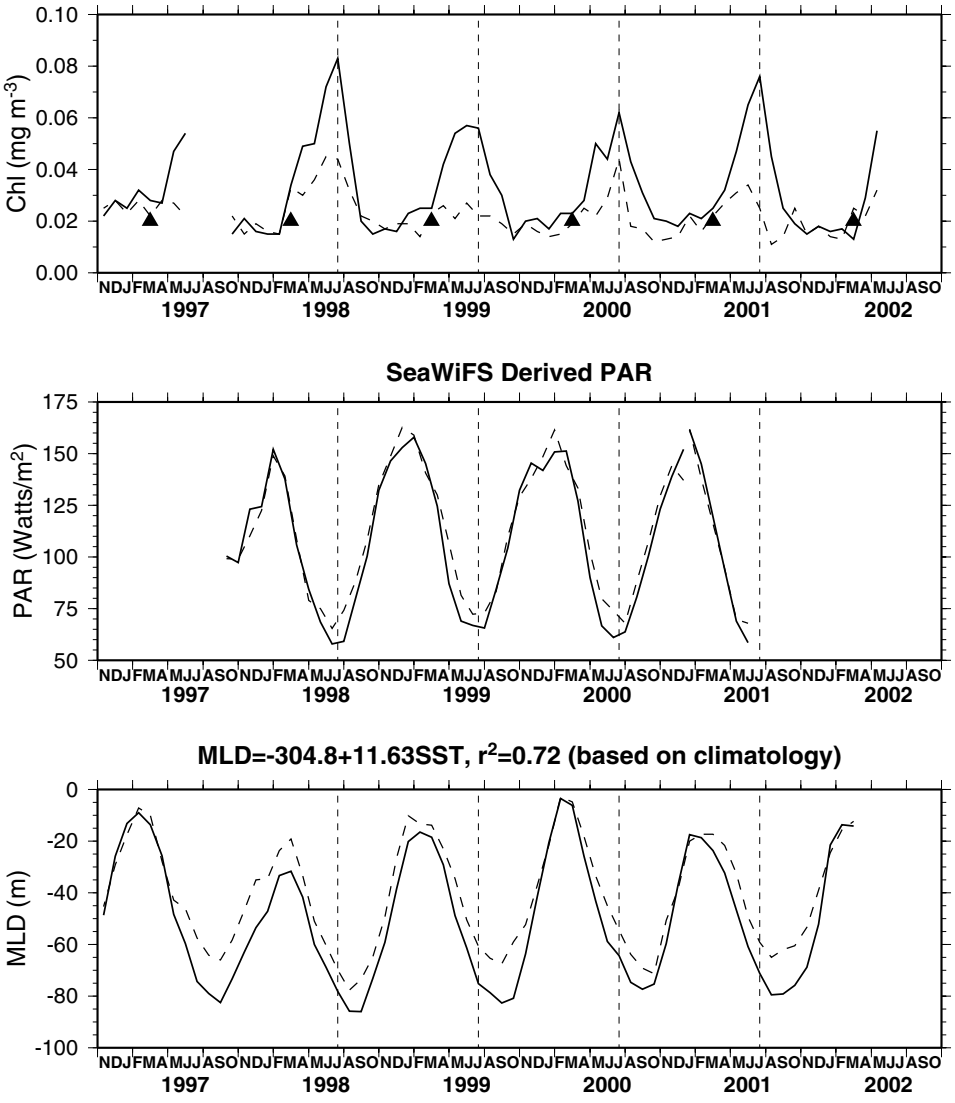

Fig. 8. Time series of OCTS (November 96 - June 97) and SeaWiFS (September 97 - January 02) chlorophyll (top), SeaWiFS-derived PAR (middle), and SST-derived mixed-layer depth (bottom) at 28^{o}S, 105^{o}W (solid lines) and at 25^{o}S, 117.5^{o}W (dashed lines). The latter location corresponds to the minimum chlorophyll concentration inside the South Pacific subtropical gyre. The triangles represent the chlorophyll concentration observed at 28^{o}S, 105^{o}W during March 1994 (Chavez *et al.*, 1995). The observed value is repeated every year for comparison.

Table 1. Cross-correlation (R) and lag in months (R/Lag[1]) between [2]A_{chl} and [3]MLD, SST, SSHA, and Ekman vertical velocity (w_e). Correlation analyses are based on a 5-year time series (Nov 96 -Sep 01)

Subtropical Gyre	A_{chl} vs. MLD	A_{chl} vs. SST	A_{chl} vs. SSHA	A_{chl} vs. w_e
North Pacific	-0.75/0	0.86/0	0.68/1	-0.61/1
South Pacific	-0.88/1	0.89/2	0.64/3	-0.45/-2
Indian Ocean	-0.84/1	0.89/2	0.61/3	+0.78/1
North Atlantic	-0.89/1	0.86/2	0.77/3	-0.65/-3
South Atlantic	-0.88/1	0.92/2	0.79/3	-0.71/-4

(1) Lag = positive values indicate A_{chl} leads, negative implies A_{chl} lags
(2) A_{chl} = Area fraction with chl ≤ 0.07 mg m^{-3}
(3) 5-year MLD time series produced from WOA94 monthly climatology

Figure 9 shows Indian Ocean SST, w_e, SeaWiFS chl-*a*, and surface currents for two 3-month periods: January through March and July through September. The surface currents are a combination of T/P-derived geostrophic currents and Ekman drift. Note the intensification of the northeastward flow along the southern boundary (white box) of the gyre in austral winter. The location of the subtropical front (STF) is marked by the dotted line using the 15°C isotherm at the surface, as the STF is marked by a strong temperature gradient between 14°C and 15.5°C (Read *et al.*, 2000). The stronger flow is accompanied by a northward displacement of the STF, downwelling intensification, and a reduction in the size of the oligotrophic region. This raises the question as to whether there is an increase in the northward flux of nutrients resulting from the flow intensification.

Table 2 summarizes the seasonal changes in physical forcing, nutrient flux, and biological response of the Indian Ocean gyre. The nitrate and phosphate fluxes were calculated using the surface currents and seasonal nutrient climatologies. The pattern seems coherent with the northward displacement of the nutrient rich STF. During the austral winter, the Indian Ocean gyre has colder SSTs, a shallower thermocline (lower SSHA), a deeper MLD, stronger downwelling, more chl-*a*, and a smaller A_{chl}. Both nitrate and phosphate northward fluxes increase in winter, which supports the hypothesis of nutrient renewal by the frontal migration.

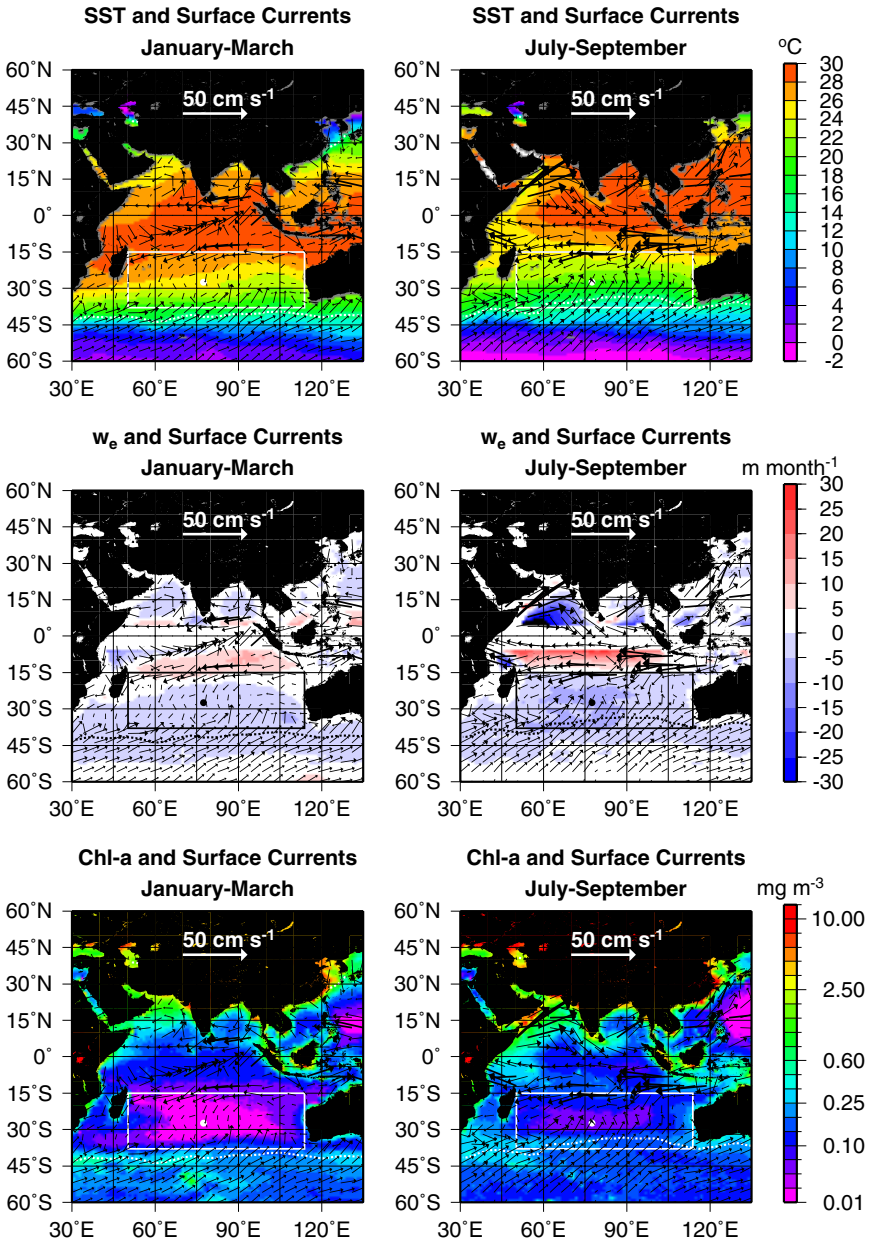

Fig. 9. Indian Ocean SST (top plates), Ekman vertical velocity (middle plates), and SeaWiFS chlorophyll (bottom plates) for January-March (left side) and July-September (right side). The surface current vectors (Ekman drift plus geostrophic) are superimposed on all fields. The dotted line between 30°S and 45°S shows the location of the subtropical front. The box delimiting the analysis regions of the Indian Ocean subtropical gyre and the location of the chlorophyll minimum concentration are provided for all variables (black for Ekman velocity and white for SST and chlorophyll).

Table 2. Seasonal variability of sea-surface temperature (SST), sea-surface height anomaly (SSHA), mixed layer depth (MLD), Ekman vertical velocity (w_e), upper 50-m northward fluxes of nitrate and phosphate (FNO_3, FPO_4) at the gyre's southern boundary, chlorophyll concentration (Chl), and size of the oligotrophic region (A_{Chl} with Chl ≤ 0.07 mg m^{-3}).

Parameter	Jan-Feb-Mar	Apr-May-Jun	Jul-Aug-Sep	Oct-Nov-Dec
SST (°C)	23.9	22.3	19.8	21.1
SSHA (cm)	1.2	0.7	-1.3	-1.5
MLD (m)	27.9	49.6	91.6	32.8
w_e (cm/d)	-1.3	-4.5	-7.2	-4.9
FNO_3 (Gmol/d)	83.6	76.6	104.0	85.3
FPO_4 (Gmol/d)	3.5	6.3	6.2	2.4
Chl (mg m^{-3})	0.09	0.13	0.14	0.11
A_{chl}	0.50	0.17	0.15	0.64

Long-term trends

Although the available ocean color record is still very short to unequivocally correlate climate variability indices to observed trends in biomass, some consistent patterns are emerging. Figure 10 shows the time series of A_{chl} for the gyres. The seasonal range is significant for all gyres and all gyres display systematic trends. The North Pacific and North Atlantic gyres have upward trends, while the Indian Ocean, South Atlantic, and South Pacific gyres have downward trends. This leads to the conclusion that the northern-hemisphere gyres are getting larger, while the southern-hemisphere gyres are getting smaller. The slopes were computed using only the first 5 years of data because the final year is incomplete by two months. The largest upward trend is in the North Atlantic, a 3.8%/year fractional size increase. The Indian Ocean has the largest downward trend, a decrease in fractional size of the oligotrophic region of about 3.3%/year. The net total change, computed as the sum of all slopes, is 0.22%.

Figure 11 shows time series of the mean chl-*a* concentration within each of the domain boxes. In cases where A_{chl} expands (Figure 10), the average chlorophyll concentration decreases (Figure 11). This is clearly shown by the opposite phases of A_{chl} and chl-*a* seasonal cycles. The amplitude of the mean chl-*a* seasonal cycles in the Indian and South Atlantic gyre domains are the largest, i.e., 0.05 to 0.12 mg m^{-3}. The amplitudes of the seasonal cycles at the locations of the climatological minimum concentration (not shown) are also largest for the Indian and South Atlantic Oceans. The long-term trends of A_{chl} and mean chl-*a* are also anticorrelated.

Table 3 summarizes the trends in A_{chl} and mean chl-*a* in %/yr for all five gyres. The mean chl-*a* trends are obtained by dividing the chl-*a* concentration trend by the mean chl-*a* of the period. Although all the gyres have an inverse correlation between their fractional size and the mean concentration, the magnitude of the A_{chl} and concentration trends are only similar in the Indian Ocean where the gyre size shows a decrease of 3.3%/yr, accompanied by a concentration increase of 3.9%/yr. In the South Atlantic, the gyre size decreases 1.4%/yr

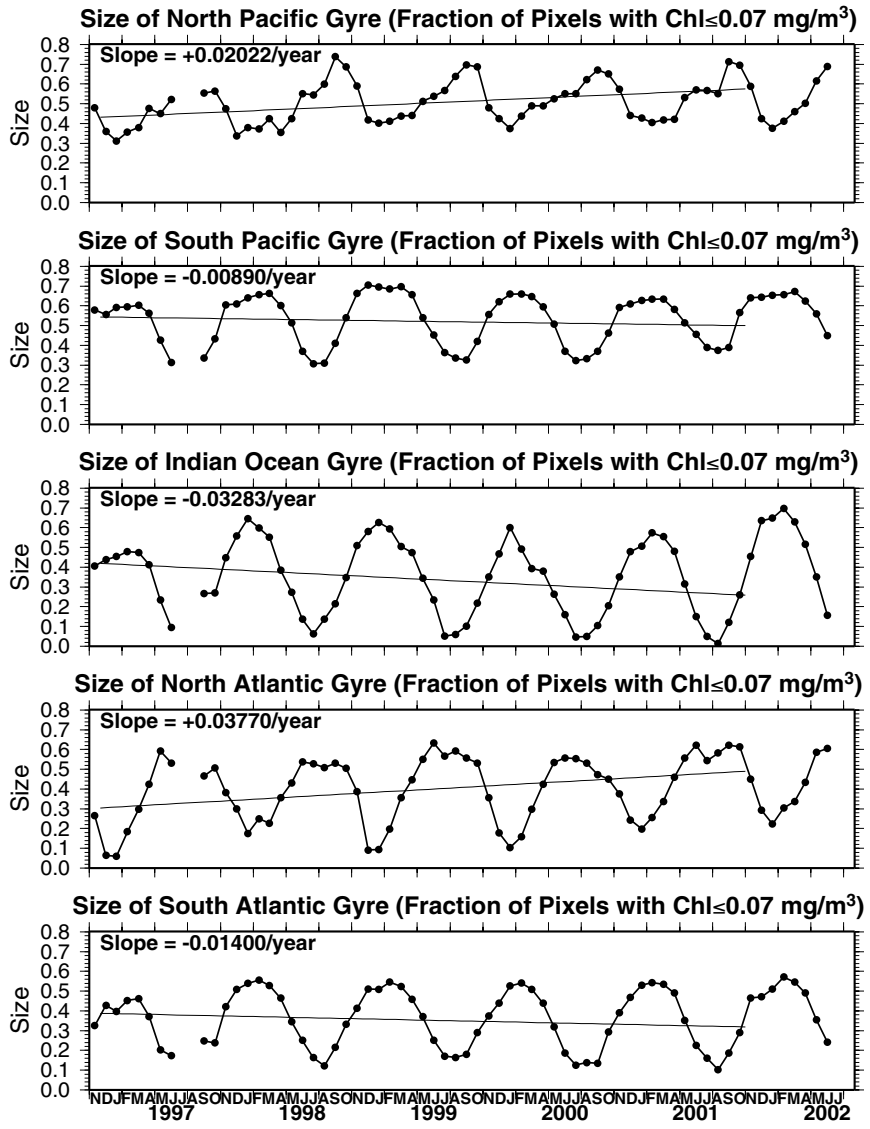

Fig. 10. Time series of the fractional size of the oligotrophic areas (chl $\leq$ 0.07 mg m^{-3}) inside the North Pacific, South Pacific, Indian Ocean, North Atlantic, and South Atlantic subtropical gyres. The values were derived from OCTS (November 96 - June 97) and SeaWiFS (September 97 - June 02) data. The linear trends are superimposed on each plot and represent five complete years of data (November 96 - October 01).

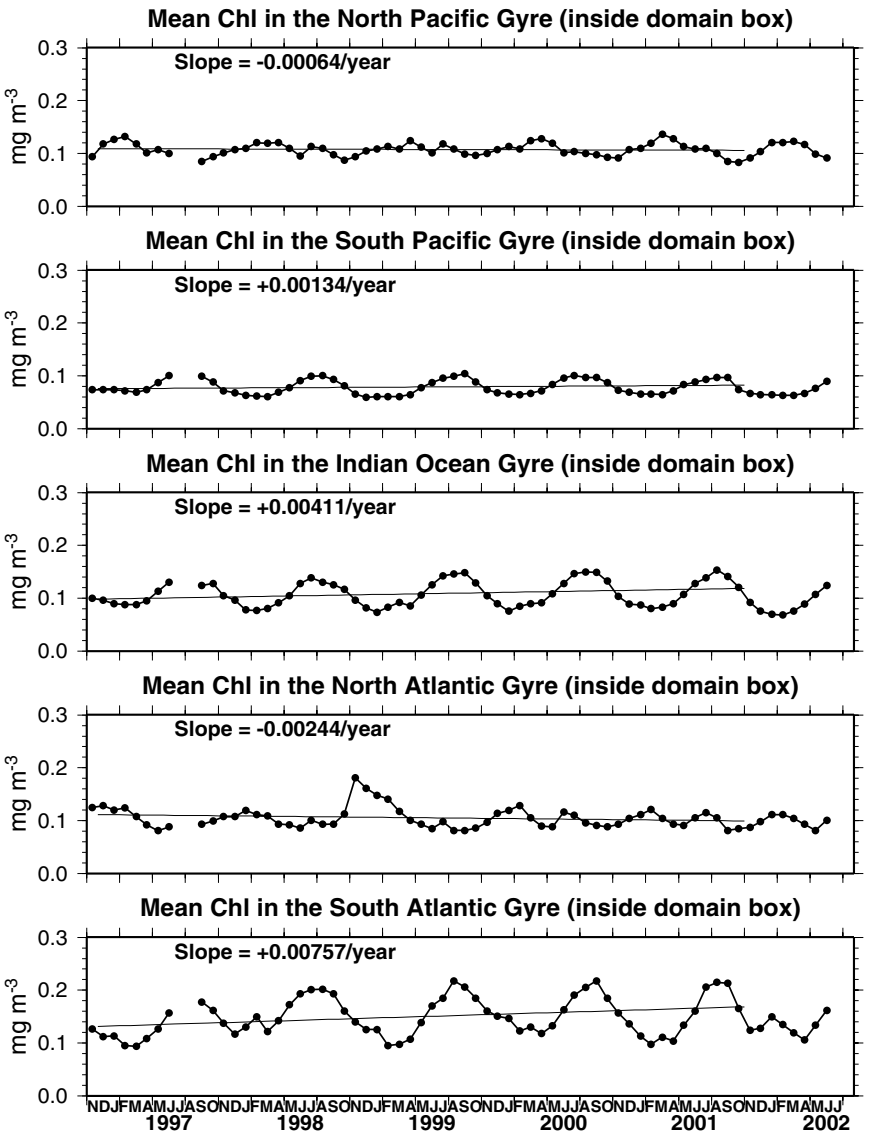

Fig. 11. Time series of mean chlorophyll concentration inside the domain boxes of the North Pacific, South Pacific, Indian Ocean, North Atlantic, and South Atlantic subtropical gyres. The values were derived from OCTS (November 96 - June 97) and SeaWiFS (September 97 - June 02) data. The linear trends are superimposed on each plot and represent five complete years of data (November 96 - October 01).

while the concentration rises at a rate of 5.1%/yr. Conversely, the North Pacific gyre increases in size by 2.0%/yr while the mean concentration decreases by 0.6%/yr. This implies that the meteorological and hydrographic factors affecting the gyre dynamics are not linearly coupled with the large-scale biogeochemical response in the subtropical gyre domains. As shown in previous sections, a combination of wind forcing, vertical mixing, thermocline displacement, and Ekman pumping are the predominant factors contributing to the observed gyre variability.

Table 3. Trends in the fractional area and mean chl-*a* concentration for the five subtropical gyres.

Gyre	A_{chl} Trend (%/yr)	Mean Chl-a Trend (%/yr)
North Pacific	+2.02	-0.59
South Pacific	-0.89	+1.72
Indian Ocean	-3.38	+3.87
North Atlantic	+3.77	-2.33
South Atlantic	-1.40	+5.11

While the limited areas selected for the gyre analyses indicate trends, the SeaWiFS Project sensor stability analyses using the derived weekly global mean normalized water leaving radiances and chl-*a* for both deep water (deeper than 1000 m) and clear water (concentrations ≤ 0.15 mg m^{-3}) regimes show no long term trends. This implies hemispheric trends in the gyre areas are indeed nearly balanced as suggested earlier.

Also, excluding the OCTS data from the time trend analysis (Table 3) does not change the sign of the trends, although the slopes are altered. The same is true for the regional mean chl-*a* trends, except that the North Pacific trend changes from slightly negative to positive. The consistency between the OCTS and SeaWiFS data can be questioned, although every effort was made by (Wang *et al.*, 2002) to ensure compatibility. In addition, the OCTS and early SeaWiFS data sets straddle the 1997-1998 El Niño-La Niña making it difficult to evaluate potential biases, especially in the OCTS data which has a shorter data record and less validation data.

Observational evidence for interannual to interdecadal variability in the intensity of ocean gyres has been previously reported. In the Indian Ocean gyre, as demonstrated earlier, nutrient enrichment is largely driven by the migration of the STF. However, there is evidence that other mechanisms may be also responsible for the downward (upward) trend in the A_{chl} of the Indian Ocean gyre. Bindoff and McDougall (2000) compared historical T and S data (median date of 1962) with a hydrographic section at a mean latitude of 32°S in October-November 1987. They estimated a decrease of the gyre rotation rate of about 20% at the depth (410-830 m) of the Sub-Antarctic Mode Water (SAMW). The estimated rotation rate change decreases almost linearly with greater depth to zero at the oxygen minimum in Indian Deep Water (IDW). The temporal difference between the synoptic and historical hydrographic data is 25±10 years, which translates into a decrease of 0.6 to 1.3% per year in the gyre rotation rate. In addition, over most of the South Indian subtropical gyre, SSTs have increased by 0.25°C since the 1950s (Bindoff and McDougall, 2000). The combined warming (increased stratification) and reduction of the gyre rotation rate (shallower pycnocline/nutricline) should

induce a biological response. However, the two effects would tend to have opposing influences on vertical nutrient fluxes.

Curry and McCartney (2001) show evidence that variability in the intensity of the North Atlantic gyre circulation is related to the NAO. The transport index, derived from the differences in potential energy anomaly between the central Labrador Basin and Bermuda, showed significant decadal variability related to the NAO. There was also an upward trend in transport during 1970-1995 of 0.8 Sv (20 Sv/25 years), which translates into 1.6%/yr increase in the strength of the gyre. This transport trend is comparable in magnitude to the 2.0%/yr upward trend in the fractional size of the oligotrophic waters inside the North Atlantic gyre. This trend correlation implies a coupling between the gyre circulation and upper-ocean nutrient supply. The positive state of the NAO index in the 1970s and 1990s reflect enhanced midlatitude westerlies, with related shifts in air-sea exchanges of heat, freshwater, and momentum (Curry and McCartney, 2001). Since the gyres are wind and buoyancy forced, the North Atlantic gyre's strength and size would be enhanced accordingly. As the gyre strengthens, the pycnocline, and, consequently, the nutricline, deepens in response to baroclinic adjustment and increased downwelling via Ekman pumping. Thus, renewal of nutrients via vertical mixing is reduced and chl-*a* concentration should diminish as a result.

Conclusions

The dynamic and biological gyre centers are not collocated. The location of the minimum chlorophyll concentration is a better indicator of the maximum nutricline depth than the location of the maximum dynamic height. Within the biological center of the gyres, photoadaptation is the most probable mechanism for chl-*a* enhancement during winter because nutrient renewal in the euphotic zone is limited due to the nutricline being much deeper than the mixed layer.

The 6-year time series of ocean color from OCTS and SeaWiFS data reveal large seasonal variability in the extent of the low chlorophyll regions of the gyres. Vertical mixing, Ekman pumping, and thermocline displacement are the main driving mechanisms for the observed seasonal changes in chlorophyll concentration.

The Indian Ocean subtropical gyre has a unique seasonal behavior in response to physical forcing. The chl-*a* concentration increases with downwelling intensification. The increase in chl-*a* coincides with the northward migration of the subtropical front in austral winter, which increases the transport of nutrients to the gyre region.

Systematic trends in chl-*a* distribution suggest that the northern hemisphere gyres are expanding and becoming more oligiotrophic, while the southern hemisphere gyres are shrinking and becoming less oligiotrophic. Although the available ocean color record is still too short to unambiguously relate these trends in biomass to climate variability, some consistent dynamic patterns related to known climate cycles (PDO, NAO, ACW) are beginning to emerge. A longer ocean record (~10 years) will be required to establish a more concrete correlation between the long-term variability of the subtropical gyres and climate trends. The exact nature of the couplings will require modeling studies in addition to the collection and analysis of longer satellite and in situ data records. The analyses presented herein are intended to simply highlight the possible connections between biological and physical variability in the subtropical gyres on seasonal and interannual time scales.

Appendix

Modes of Climate Variability and Marine Ecosystem Response

The PDO is the leading mode of October-March SST variability poleward of 20°N in the North Pacific (Mantua *et al.*, 1997). The essence of the PDO climate signature is the coherent, interdecadal timescale of ocean sea surface temperature (SST) -atmospheric sea level pressure (SLP) covariance. The PDO is correlated with indices commonly used to monitor the atmospheric and oceanic aspects of ENSO (Mantua *et al.*, 1997): the Southern Oscillation Index (SOI) and the Cold Tongue Index (CTI, the average SST anomaly from 6°N to 6°S, 180°W to 90°W), respectively. The SOI and CTI are correlated with the PDO in such a way that warm- (cold-) phase ENSO-like conditions tend to coincide with the years of positive (negative) polarity in the PDO, albeit fluctuations in the CTI are mostly interannual, while those in the PDO are predominantly interdecadal (Mantua *et al.*, 1997). Significant PDO polarity reversals, or regime shifts, occurred in 1925, 1947, and 1977 (Mantua *et al.*, 1997). A shift in phytoplankton community structure, and other related biogeochemical processes, has been hypothesized for the upper portion of the North Pacific subtropical gyre during the past several decades as a result of ENSO-PDO interactions (Karl *et al.*, 2001).

The NAO is a pressure seesaw between the Azores high and the Icelandic low and is most prominent in boreal winter (Hastenrath and Greischar, 2001). The NAO index may be defined as the difference in pressure at Ponta Delgada, Azores, minus that at Akureyri, Iceland (Rogers, 1984; 1985). A consequence of a positive (negative) NAO index is the strengthening (weakening) of the westerlies (Portis *et al.*, 2001). During high NAO winters, the westerlies over Europe are more than 8 m s^{-1} stronger than during low NAO winters (Hurrell, 1995). The NAO is not a purely random process, nor does it exhibit a clear mode of oscillation. The autocorrelation in the index time series shows intermittent quasi-biennial (2.5 years) and quasi-decadal (6 to 10 years) oscillations that have an impact on the North Atlantic atmosphere-ocean coupled system (Wanner *et al.*, 2001). Long-term evolutions in upper-air circulation, near-surface wind pattern, and SST over the recent 40-yr period are in tune with a trend toward greater prevalence of the positive-NAO phase (Hastenrath and Greischar, 2001).

The NAO may be seen as a proxy for regulating forces in aquatic and terrestrial ecosystems, with ecological responses in timing of reproduction, population dynamics, abundance, spatial distribution and inter-specific relationships such as competition and predator-prey relationships (Ottersen *et al.*, 2001). The NAO affects the ecosystems of the NE and NW Atlantic shelves, as well as the biogeochemical processes of the North Atlantic subtropical gyre. In the NE Atlantic, the NAO influences phytoplankton standing stock by regulating mixed layer depth (MLD), thereby affecting the onset of the spring bloom and subsequent levels of primary production (Greene and Pershing, 2000). In the NW Atlantic, ecosystem changes due to the NAO are in response to variability of upper-ocean circulation and water mass distribution (Greene and Pershing, 2000). A study of the effects of the NAO positive phase swing between the 1960s and 1990s (Oschlies, 2001) in the North Atlantic subtropical gyre, using a coupled ecosystem-circulation model, demonstrated a decrease of nitrate supply by about 30% near Bermuda and in mid-latitudes. The nitrate supply decrease is a result of shallower winter mixed layers (20 to 100 m), reflecting an anomalous heat gain by up to 20 W m^{-2}. The transition region from the oligotrophic subtropical gyre to the eutrophic

regions surrounding it is most sensitive to NAO-related climate fluctuations; in this region even small changes in the depth of winter mixing can determine whether the mixed layer penetrates the nutricline (Oschlies, 2001).

The ACW has its major source in the western subtropical South Pacific where interannual anomalies in SST and preciptable water form (Peterson and White, 1998). Once established, these interannual anomalies, in tandem with anomalies in SLP, move south toward the Southern Ocean and migrate eastward around the globe through a combination of oceanic advection with Antarctic Circumpolar Current (ACC) and ocean-atmosphere coupling. It takes 8-10 years for the wave pattern to circle Antarctica. Large portions of the interannual SST anomalies advect northward into the South Atlantic and Indian Oceans, ultimately reaching the tropics in each basin 6-8 years after appearing in the low-latitude Pacific. Jacobs and Mitchell (1996) showed persistent SSH, wind stress curl (WSC), and SST anomalies propagating eastward about the Antarctic continent consistent with the ACW behavior. During the observation time period (1986-1996), the SSH appeared quasi-periodic with a dominant 4 year period and 180^{o} longitude wavelength. The WSC anomalies were about 45^{o} longitude farther east than the SSH anomalies, with the WSC leading SSH by about 1/4 cycle. The SSH and SST were in phase. The ocean circulation variations implied by the SSH anomalies have implications for possible dynamics that may be coupled with the SST anomalies (Jacobs and Mitchell, 1996). The zonal SSH gradients imply meridional transports that advect the large scale mean temperature field. Thus, the ACW may have an impact on the position of the subtropical front (STF), which may, in turn, affect advective fluxes into the gyre regions. The passage of the ACW, with its associated change in SST and MLD, also substantially affects the regional rates of gas exchange, vertical mixing, and biological export of carbon (Le Quere *et al.*, 2000; Louanchi and Hoppema, 2000).

References

Barnes, R.A., Eplee, R.E., Jr., Patt, F.S., McClain, C.R., 1999. Changes in the radiometric sensitivity of SeaWiFS. Appl. Optics 38, 4649-4664.

Barnes, R.A., Eplee, R.E., Jr., Schmidt, G.M., Patt, F.S., McClain, C.R., 2001. The calibration of SeaWiFS, Part 1: Direct techniques. Appl. Optics 40, 6682-6700.

Bindoff, N.L., McDougall, T.J., 2000. Decadal changes along an Indian ocean section at 32 degrees S and their interpretation. Journal of Physical Oceanography 30, 1207-1222.

Chavez, F.P., Buck, K.R., Bidigare, R.R., Karl, D.M., Hebel, D., Latasa, M., Campbell, L., Newton, J., 1995. On the Chlorophyll-a Retention Properties of Glass-Fiber Gf/F Filters. Limnology and Oceanography 40, 428-433.

Chen, T.C., Pfaendtner, J., Weng, S.P., 1994. Aspects of the Hydrological Cycle of the Ocean-Atmosphere System. Journal of Physical Oceanography 24, 1827-1833.

Curry, R.G., McCartney, M.S., 2001. Ocean gyre circulation changes associated with the North Atlantic Oscillation. Journal of Physical Oceanography 31, 3374-3400.

Eplee, R.E., Jr., Robinson, W.D., Bailey, S.W., Clarke, D.K., Werdell, P.J., Wang, M., Barnes, R.A., McClain, C.R., 2001. The calibration of SeaWiFS, Part 2: Vicarious techniques. Appl. Optics 40, 6701-6718.

Greene, C.H., Pershing, A.J., 2000. The response of Calanus finmarchicus populations to climate variability in the Northwest Atlantic: basin-scale forcing associated with the North Atlantic Oscillation. Ices Journal of Marine Science 57, 1536-1544.

Hastenrath, S., Greischar, L., 2001. The North Atlantic oscillation in the NCEP-NCAR reanalysis. Journal of Climate 14, 2404-2413.

Hayward, T.L., 1987. The Nutrient Distribution and Primary Production in the Central North Pacific. Deep-Sea Research Part a-Oceanographic Research Papers 34, 1593-1627.

Hayward, T.L., 1991. Primary production in the North Pacific Central Gyre: A controversy with important implications. Trends Ecol. Evol. 6, 281-284.

Huang, R.X., Russell, S., 1994. Ventilation of the Subtropical North Pacific. Journal of Physical Oceanography 24, 2589-2605.

Huang, R.X., Qiu, B., 1994. Three-Dimensional Structure of the Wind-Driven Circulation in the Subtropical North Pacific. Journal of Physical Oceanography 24, 1608-1622.

Hurrell, J.W., 1995. Decadal Trends in the North-Atlantic Oscillation - Regional Temperatures and Precipitation. Science 269, 676-679.

Jacobs, G.A., Mitchell, J.L., 1996. Ocean circulation variations associated with the Antarctic circumpolar wave. Geophysical Research Letters 23, 2947-2950.

Jenkins, W.J., Goldman, J.C., 1985. Seasonal Oxygen Cycling and Primary Production in the Sargasso Sea. Journal of Marine Research 43, 465-491.

Jones, D.R., Karl, D.M., Laws, E.A., 1996. Growth rates and production of heterotrophic bacteria and phytoplankton in the North Pacific subtropical gyre. Deep-Sea Research Part I-Oceanographic Research Papers 43, 1567-1580.

Karl, D.M., Lukas, R., 1996. The Hawaii Ocean Time-series (HOT) program: Background, rationale and field implementation. Deep-Sea Res. II 43, 129-156.

Karl, D.M., Bidigare, R.R., Letelier, R.M., 2001. Long-term changes in plankton community structure and productivity in the North Pacific Subtropical Gyre: The domain shift hypothesis. Deep-Sea Res. II 48, 1449-1470.

Karl, D.M., Christian, J.R., Dore, J.E., Hebel, D.V., Letelier, R.M., Tupas, L.M., Winn, C.D., 1996. Seasonal and interannual variability in primary production and particle flux at Station ALOHA. Deep-Sea Res. II 43, 539-568.

Kleeman, R., Naik, N.H., Cane, M.A., 2000. Meridional location of the Pacific ocean subtropical gyre. Journal of Physical Oceanography 30, 1988-2000.

Laws, E.A., Ditullio, G.R., Redalje, D.G., 1987. High Phytoplankton Growth and Production-Rates in the North Pacific Subtropical Gyre. Limnology and Oceanography 32, 905-918.

Le Quere, C., Orr, J.C., Monfray, P., Aumont, O., Madec, G., 2000. Interannual variability of the oceanic sink of CO2 from 1979 through 1997. Global Biogeochemical Cycles 14, 1247-1265.
Louanchi, F., Hoppema, M., 2000. Interannual variations of the Antarctic Ocean CO2 uptake from 1986 to 1994. Marine Chemistry 72, 103-114.
Mantua, N.J., Hare, S.R., Zhang, Y., Wallace, J.M., Francis, R.C., 1997. A Pacific interdecadal climate oscillation with impacts on salmon production. Bulletin of the American Meteorological Society 78, 1069-1079.
Marañón, E., Holligan, P.M., Varela, M., Mouriño, B., Bale, A.J., 2000. Basin-scale variability of phytoplankton biomass, production and growth in the Atlantic Ocean. Deep-Sea Res. I 47, 825-857.
Marra, J., Heinemann, K.R., 1987. Primary Production in the North Pacific Central Gyre - Some New Measurements Based on C-14. Deep-Sea Research Part a-Oceanographic Research Papers 34, 1821-1829.
Morris, M., Roemmich, D., Cornuelle, B., 1996. Observations of variability in the South Pacific subtropical gyre. Journal of Physical Oceanography 26, 2359-2380.
Oschlies, A., 2001. NAO-induced long-term changes in nutrient supply to the surface waters of the North Atlantic. Geophysical Research Letters 28, 1751-1754.
Ottersen, G., Planque, B., Belgrano, A., Post, E., Reid, P.C., Stenseth, N.C., 2001. Ecological effects of the North Atlantic Oscillation. Oecologia 128, 1-14.
Pedlosky, J., 1990. The Dynamics of the Oceanic Subtropical Gyres. Science 248, 316-322.
Peterson, R.G., White, W.B., 1998. Slow oceanic teleconnections linking the Antarctic Circumpolar Wave with the tropical El Nino-Southern Oscillation. Journal of Geophysical Research-Oceans 103, 24573-24583.
Portis, D.H., Walsh, J.E., El Hamly, M., Lamb, P.J., 2001. Seasonality of the North Atlantic oscillation. Journal of Climate 14, 2069-2078.
Read, J.F., Lucas, M.I., Holley, S.E., Pollard, R.T., 2000. Phytoplankton, nutrients and hydrography in the frontal zone between the Southwest Indian Subtropical gyre and the Southern Ocean. Deep-Sea Research Part I-Oceanographic Research Papers 47, 2341-2368.
Reynolds, R.W., Smith, T.M., 1994. Improved Global Sea-Surface Temperature Analyses Using Optimum Interpolation. Journal of Climate 7, 929-948.
Rogers, J.C., 1984. The Association between the North-Atlantic Oscillation and the Southern Oscillation in the Northern Hemisphere. Monthly Weather Review 112, 1999-2015.
Rogers, J.C., 1985. Atmospheric Circulation Changes Associated with the Warming over the Northern North-Atlantic in the 1920s. Journal of Climate and Applied Meteorology 24, 1303-1310.
Turk, D., McPhaden, M.J., Busalacchi, A.J., Lewis, M.R., 2001. Remotely sensed biological production in the equatorial Pacific. Science 293, 471-474.
Wang, M., Isaacman, A., Franz, B., McClain, C.R., 2002. Ocean color optical property data derived from the Japanese Ocean Color and Temperature Scanner and the French Polarization and Directionality of the Earth's Reflectance: a comparison study. Appl. Optics 41, 974-990.
Wanner, H., Bronnimann, S., Casty, C., Gyalistras, D., Luterbacher, J., Schmutz, C., Stephenson, D.B., Xoplaki, E., 2001. North Atlantic Oscillation - Concepts and studies. Surveys in Geophysics 22, 321-382.
Winn, C.D., Campbell, L., Christian, J.R., Letelier, R.M., Hebel, D.V., Dore, J.E., Fujieki, L., Karl, D.M., 1995. Seasonal Variability in the Phytoplankton Community of the North Pacific Subtropical Gyre. Global Biogeochemical Cycles 9, 605-620.
Wyrtki, K., Meyers, G., 1976. Trade Wind Field over Pacific Ocean. Journal of Applied Meteorology 15, 698-704.

REPORT DOCUMENTATION PAGE

Form Approved
OMB No. 0704-0188

1. AGENCY USE ONLY *(Leave blank)*	2. REPORT DATE	3. REPORT TYPE AND DATES COVERED
	September 2002	Technical Memorandum

4. TITLE AND SUBTITLE
Subtropical Gyre Variability Observed by Ocean Color Satellites

5. FUNDING NUMBERS
Code 970

6. AUTHOR(S)
C.R. McClain, S.R. Signorini, J.R. Christian

7. PERFORMING ORGANIZATION NAME(S) AND ADDRESS (ES)
Goddard Space Flight Center
Greenbelt, Maryland 20771

8. PEFORMING ORGANIZATION REPORT NUMBER
2002-03502-0

9. SPONSORING / MONITORING AGENCY NAME(S) AND ADDRESS (ES)
National Aeronautics and Space Administration
Washington, DC 20546-0001

10. SPONSORING / MONITORING AGENCY REPORT NUMBER
TM-2002-211616

11. SUPPLEMENTARY NOTES
S.R. Signorini, Science Applications International Corporation, Beltsville, MD
James R. Christian, Earth System Science Interdisciplinary Center, University of Maryland, College Park, MD

12a. DISTRIBUTION / AVAILABILITY STATEMENT
Unclassified–Unlimited
Subject Category: 42
Report available from the NASA Center for AeroSpace Information,
7121 Standard Drive, Hanover, MD 21076-1320. (301) 621-0390.

12b. DISTRIBUTION CODE

13. ABSTRACT *(Maximum 200 words)*

The subtropical gyres of the world are extensive, coherent regions that occupy about 40% of the surface of the earth. Once thought to be homogeneous and static habitats, there is increasing evidence that mid-latitude gyres exhibit substantial physical and biological variability on a variety of time scales. While biological productivity within these oligotrophic regions may be relatively small, their immense size makes their total contribution significant. Global distributions of dynamic height derived from satellite altimeter data, and chlorophyll concentration derived from satellite ocean color data, show that the dynamic center of the gyres, the region of maximum dynamic height where the thermocline is deepest, does not coincide with the region of minimum chlorophyll concentration. The physical and biological processes by which this distribution of ocean properties is maintained, and the spatial and temporal scales of variability associated with these processes, are analyzed using global surface chlorophyll-a concentrations, sea surface height, sea surface temperature and surface winds from operational satellite and meteorological sources, and hydrographic data from climatologies and individual surveys. Seasonal and interannual variability in the areal extent of the subtropical gyres are examined using 8 months (November 1996 - June 1997) of OCTS and nearly 5 years (September 1997 - June 02) of SeaWiFS ocean color data and are interpreted in the context of climate variability and measured changes in other ocean properties (i.e., wind forcing, surface currents, Ekman pumping, and vertical mixing). The North Pacific and North Atlantic gyres are observed to be shrinking over this period, while the South Pacific, South Atlantic, and South Indian Ocean gyres appear to be expanding.

14. SUBJECT TERMS
subtropical gyres, ocean, SeaWIFS, South Pacific, North Pacific, Indian Ocean, South Atlantic, North Atlantic

15. NUMBER OF PAGES
26

16. PRICE CODE

17. SECURITY CLASSIFICATION OF REPORT	18. SECURITY CLASSIFICATION OF THIS PAGE	19. SECURITY CLASSIFICATION OF ABSTRACT	20. LIMITATION OF ABSTRACT
Unclassified	Unclassified	Unclassified	UL